Concerning the equilibrium sequences of binary star systems, we have summarized classical results of incompressible ellipsoidal configurations. Recent results of compressible binary star systems obtained by the ellipsoidal approximation and by numerical computations have been shown and discussed. It is important to note that numerical computational solutions to *exact equations* show that compressibility may lead realistic neutron star binary systems to mass overflows instead of dynamical disruptions for a wide range of parameters.

Darwin-Riemann Problems in Newtonian Gravity

Yoshiharu ERIGUCHI[1,*] and Kōji URYŪ[2,**]
[1]*Department of Earth Science and Astronomy*
Graduate School of Arts and Sciences, University of Tokyo
Komaba, Meguro, Tokyo 153-8902, Japan
[2]*SISSA, Via Beirut 2/4, Trieste 34013, Italy*

(Received)

§1. Quasi-equilibrium stage of evolution of compact binary star systems

1.1. *Time scales and classification of evolutionary stages of compact binary star systems*

As is well known, gravitational waves from compact binary star systems will carry away the angular momentum and energy from the systems. It implies that the binary star system will necessarily evolve to shrink its orbital radius and that eventually merging of two compact component stars will occur. There are three typical time scales to classify such an evolution: 1) the rotational period, $\tau_{\rm rot}$, 2) the time scale of the orbital change due to gravitational wave emission, $\tau_{\rm GW}$, and 3) the light crossing time scale of the system, $\tau_{\rm dyn}$.

Let us consider a binary system consisting of two stars with masses M_1 and M_2. Two stars are in a circular orbit with a separation of $A \equiv 2d$. Here the separation of the binary system is defined by the distance between two centers of mass of two stars. If stars are point masses with the same mass and the quadrupole formula for the gravitational radiation reaction is used, time scales mentioned above can be estimated as follows in Newtonian gravity:

$$\tau_{\rm dyn} \equiv d \quad , \tag{1·1}$$

$$\tau_{\rm GW} \equiv \left(\frac{1}{A}\frac{dA}{dt}\right)^{-1} \approx \frac{5}{8}\left(\frac{M}{R_*}\right)^{-3}\left(\frac{d}{R_*}\right)^{3} \quad , \tag{1·2}$$

$$\tau_{\rm rot} \equiv \frac{2\pi}{\Omega} \approx 4\pi\left(\frac{M}{R_*}\right)^{-1/2}\left(\frac{d}{R_*}\right)^{1/2} \quad , \tag{1·3}$$

where R_* and Ω are the radius of the star and the angular velocity, respectively, and geometrized units $c = G = 1$ are used. If we specify the value of the compactness M/R_*, we can evaluate these time scales as shown in Table I and Fig. 1. In Table I ratios of time scales, the rotational velocity $v_{\rm rot}$ and the number of rotations during the time scale $\tau_{\rm GW}$, N, are shown for two cases of the compactness M/R_*. In Fig. 1, the ratios of time scales are plotted against the separation normalized by the stellar radius.

As seen from Table I and Fig. 1, since the time scales vary considerably as a function of the separation, we can divide the evolution of binary star systems due to

*) E-mail address: eriguchi@valis.c.u-tokyo.ac.jp
**) E-mail address: uryu@sissa.it

Table I. Ratios of time scales, the rotational velocity $v_{\rm rot}$ and the number of rotations, N, during $\tau_{\rm GW}$ at the distance of several stellar radii for different compactness parameters.

M/R_*	d/R_*	$\tau_{\rm GW}/\tau_{\rm dyn}$	$\tau_{\rm rot}/\tau_{\rm dyn}$	$v_{\rm rot}/c$	N
0.1	3.0	1.7E4	6.9E1	0.09	250
	2.0	5.0E3	5.6E1	0.11	90
	1.0	6.3E2	4.0E1	0.16	16
0.2	3.0	2.1E3	4.9E1	0.13	42
	2.0	6.3E2	4.0E1	0.16	16
	1.0	7.8E1	2.8E1	0.22	3

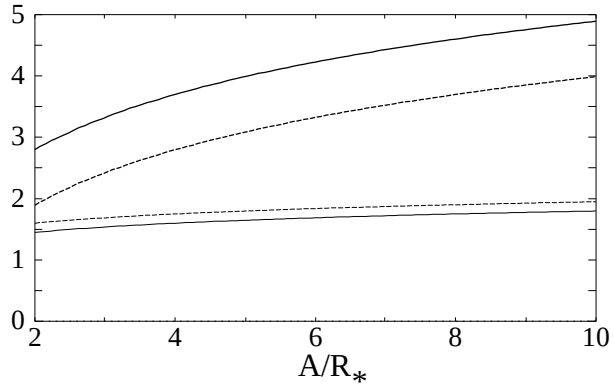

Fig. 1. Ratios of time scales $\log(\tau_{\rm GW}/\tau_{\rm dyn})$ (thick curves) and $\log(\tau_{\rm rot}/\tau_{\rm dyn})$ (thin curves) are plotted against the separation normalized by the stellar radius for two values of M/R_*. $M/R_* = 0.1$ (solid curves) and 0.2 (dashed curves).

gravitational wave emission into three distinct stages: 1) the quasi-equilibrium stage where $\tau_{\rm GW} \gg \tau_{\rm rot}$ or $d \gtrsim R_*$, 2) the merging stage where $\tau_{\rm GW} \sim \tau_{\rm rot}$ or $d \sim R_*$, and 3) a neutron star or a black hole formation stage where at first $\tau_{\rm GW} \sim \tau_{\rm rot}$ or $d \sim R_*$ and later $\tau_{\rm GW} \gtrsim \tau_{\rm rot}$ or $d \lesssim R_*$. In stage 1, gravitational wave emission hardly affects the orbital motion during several rotational periods, while in stages 2 and 3 an appreciable change of the orbital motion and/or configuration occurs in one or less orbital period or on a dynamical time scale.

Therefore, hydrodynamical simulations are most appropriate for investigations of stages 2 and 3 but not for stage 1. For stage 1, it is proper to assume that binary stars are in quasi-equilibrium states because there is little change of the configuration and the orbital motion of the binary star system. Moreover, we need to take the structure of the stars into account for the state with rather small separations $d/R_* \lesssim 2$ where this quasi-equilibrium approach may be still applied. Evolution of a binary star system in this stage is well approximated by an equilibrium sequence of a binary with a *finite size*, if we take account of proper constraints in construction of the sequence.

1.2. *Evolution of velocity fields and equilibrium sequences*

One equilibrium state of a binary star system can be specified by the following quantities: 1) masses of the stars, 2) the value of the separation, 3) the equation of state and 4) rotation laws of the stars including the internal motions.

Concerning the first two, we can freely choose those values. Although the equation of state for the realistic neutron star matter has not been fully understood for the high

density region above the nuclear density, we will be able to try several sets of equations of state.

However, it is not easy to specify the rotation law for binary star systems because the rotation law depends on the initial state, the physical state of the matter, the evolutionary time and so on. In this paper, we will consider two extreme cases for viscosity: 1) strong viscosity and 2) weak viscosity. If the effect of viscosity is strong enough, the internal flow would synchronize with the orbital rotation. On the other hand, if it is weak, the initial state of the flow would be maintained.

As Kochanek[1)] and Bildsten and Cutler[2)] have shown, the situation for neutron stars becomes very simple. The effect of viscosity for realistic neutron stars is so small that it may not affect the rotation law of binary neutron star systems. This implies that the vorticity of the neutron star system is conserved during evolution because the radiation reaction force due to gravitational wave emission is the potential force at the leading order.

Furthermore, since values of the angular velocity and the vorticity, ζ, of neutron stars will increase as the orbit shrinks, the following relations will be established at the final state of the quasi-equilibrium stage:

$$|\Omega_f| \gg |\Omega_i|, \quad |\zeta_i| \quad , \tag{1·4}$$

$$|\zeta_f| \gg |\Omega_i|, \quad |\zeta_i| \quad , \tag{1·5}$$

where quantities with suffix $_i$ or $_f$ denote those at the initial state or at the final state, respectively. Here ζ_i and ζ_f are the vorticities in the rotating frame. Since the vorticity in the inertial frame ζ_0 is conserved, we can obtain the following relation:

$$|\zeta_0| \ll |\Omega_f|, \quad |\zeta_f| \quad . \tag{1·6}$$

This means that the vorticity in the inertial frame can be considered to be negligibly small compared with the angular velocity and the vorticity in the rotating frame at the final state of the quasi-equilibrium evolution stage. In other words, we may consider that flow fields of binary neutron star systems can be regarded to be *irrotational*.

Therefore, in this paper, we will treat two extreme cases: 1) synchronously rotating binary star systems and 2) irrotational binary star systems.

In principle, we can obtain equilibrium sequences by connecting equilibrium states with the specified rotation law. However, in order to follow quasi-stationary evolution of binary star systems due to gravitational wave emission by making use of a quasi-equilibrium sequence, we need to consider conserved quantities during evolution. For binary neutron star systems, one conserved quantity is of course the vorticity in the inertial frame as mentioned above. For binary star systems emitting gravitational waves, the baryon number or the baryon mass is the second conserved quantity because matter does neither flow out from nor flow into the system. Therefore, we can construct equilibrium sequences by connecting equilibrium states with the same baryon mass and use them as quasi-stationary evolution sequences due to gravitational wave emission.

1.3. *Characteristic feature of equilibrium sequences*

Equilibrium sequences can be characterized by several sets of physical quantities such as the total angular momentum – separation relation, the angular velocity – separation relation, the energy – separation relation and so on. In this paper, we will

choose the total angular momentum – separation relation as the typical relation which reflects the essential feature of the equilibrium sequence or, in other words, of the quasi-stationary evolution sequence of the binary star system due to gravitational wave emission.

In order to show the characteristic feature of the equilibrium sequence, we will assume that masses of two stars are the same and that the stars rotate in a circular orbit. The total angular momentum $J_{\rm tot}$ is divided into two parts as follows:

$$J_{\rm tot} = J_{\rm orb} + J_{\rm spin} \quad , \tag{1·7}$$

where $J_{\rm orb}$ and $J_{\rm spin}$ are the orbital angular momentum and the spin angular momentum, respectively. If we assume that the stars are congruent, they are expressed as:

$$J_{\rm orb} = \frac{1}{4}(2M)^{3/2}A^{1/2} \quad , \tag{1·8}$$

$$J_{\rm spin} = 2(2M)^{1/2}IA^{-3/2} + 2\int \rho r \sin\theta v_\varphi d^3r \quad , \tag{1·9}$$

$$J_{\rm tot} = \frac{1}{4}(2M)^{3/2}A^{1/2} + 2(2M)^{1/2}IA^{-3/2} + 2\int \rho r \sin\theta v_\varphi d^3r \quad , \tag{1·10}$$

where we have used the relation

$$\Omega^2 A^3 = 2M \quad . \tag{1·11}$$

Here I, ρ and v_φ are the moment of inertia, the density and the φ-component of the internal velocity of the component star in the rotating frame, respectively, and (r, θ, φ) are the coordinates whose origin coincides with the center of mass of the component star.

From these expressions, we can see the dependency of the angular momentum on the separation as well as on the internal structure of the star. First, as the separation decreases, the orbital angular momentum decreases as $A^{1/2}$, while the spin angular momentum increases as $A^{-3/2}$. Second, the internal structure of the finite-size star is reflected in the second and third terms of $J_{\rm tot}$ through I and v_φ. The moment of inertia depends on the matter distribution which is governed by its self-gravity, the tidal force from the companion star, the orbital motion, the internal flow including rotation and the equation of state. The internal velocity v_φ is determined from the initial state and evolution of the velocity field.

The first feature implies that there can exist a minimum angular momentum state for a certain value of the separation, say $A_{\rm min}$. From the second feature the effect of the internal structure changes the spin angular momentum but keeps the orbital angular momentum unchanged. In particular, the change of the moment of inertia will result in the shift of the value of $A_{\rm min}$ because the moment of inertia affects through the term which behaves as $A^{-3/2}$. Thus, if I increases (decreases), $A_{\rm min}$ becomes larger (smaller). The effect of the internal flow is not so drastic. If we consider the velocity field which flows in the counter direction with respect to the orbital motion, i.e. $v_\varphi < 0$, the spin angular momentum is decreased almost evenly for all separations so that the total angular momentum decreases but the position of $A_{\rm min}$ is hardly shifted. These features are shown in Figs. 2 and 3.

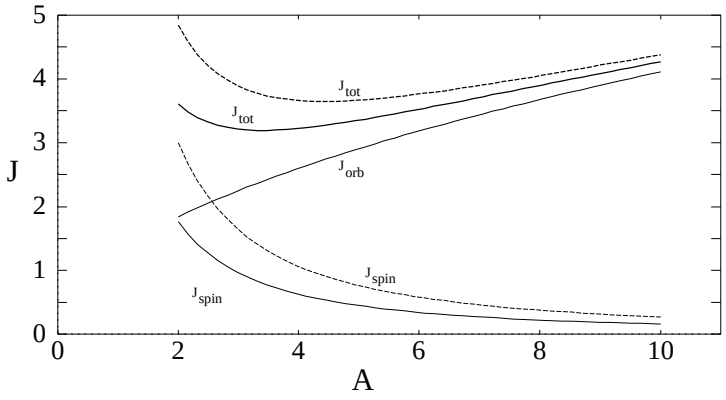

Fig. 2. Schematic figure of the angular momentum J – separation A relation. The effect of the moment of inertia is shown. Thin solid curves correspond to $J_{\rm orb}$ and $J_{\rm spin}$ and thick solid curve to $J_{\rm tot}$ for a certain value of I. Dashed curves correspond to those for larger I.

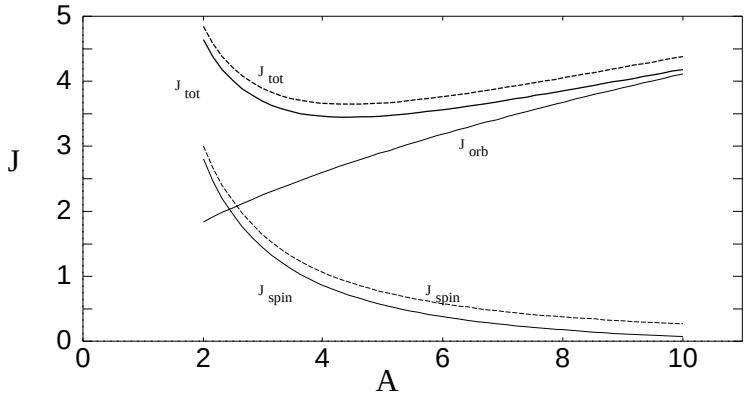

Fig. 3. Same as Fig. 2 but for the effect of the internal velocity. Dashed curves correspond to the sequence without internal velocity fields. Solid curves are those for models with internal velocity $v_\varphi < 0$.

§2. Critical states along the equilibrium sequence of binary star systems

When we consider evolutionary sequences of binary star systems, it is important to know whether each model along the sequences is stable or not against a certain kind of perturbations. If some kind of instability sets in at some point, equilibrium configurations beyond that point do not exist in realistic situations. Even if instability does not occur, at some stage there may occur some kind of significant change of configurations. In this section we will discuss such kind of critical states which will appear along evolutionary sequences.

2.1. *Contact state for congruent stars*

For congruent stars, if the separation decreases, it is most probable that two binary stars come to contact by considering the symmetry of configurations in equilibrium states. In order to find this critical state, we need to treat deformation of configurations very accurately. We will use A_c or d_c for the separation of this contact phase or the half of the separation, respectively. After this contact phase, its configuration is no more a

binary state but a single body is formed.

2.2. *Roche lobe filling state (cusp formation state)*

If masses of two stars are different or if configurations of two stars are different such as a black hole – neutron star system or if there exist internal motions, decrease of the separation results in a Roche lobe filling state. Here we use the word "Roche lobe" in its generalized sense because models can include internal flows. Since there is a cusp point on the surface of the Roche lobe, a cusp shape appears on the stellar surface, too. This state is denoted by the separation $A_{\rm OF}$ or the half of the separation $d_{\rm OF}$. Here the subscript $_{\rm OF}$ denotes that the mass begins to overflow from the Roche lobe filling star to the other star.

2.3. *Roche limit state (minimum separation state)*

The Roche limit is defined as the minimum separation for a binary system. Within the Roche limit there are no equilibrium states for the component stars. For a spherical star, the Roche limit state coincides with the state at the maximum angular velocity. However, if we take deformation of stars into account, this is no more the case. For some binary configurations, equilibrium states with larger angular velocity than that of the Roche limit state can exist. The Roche limit and its half distance are denoted as $A_{\rm RL}$ and $d_{\rm RL}$, respectively.

2.4. *Turning point of equilibrium sequence*

As discussed before, along the equilibrium sequence of binary star systems, there may appear a state where the total angular momentum becomes minimum. Since gravitational waves carry away the angular momentum from the system, the minimum state of the angular momentum denotes a critical state for equilibrium sequences. For synchronously rotating binary star sequences, this state corresponds to the onset of *secular instability* due to viscosity. On the other hand, for irrotational binary star sequences, *dynamical instability* of the orbital motion sets in at this point. We will use $A_{\rm dyn}$ and $d_{\rm dyn}$ for the separation and the half of it at this state, respectively.

2.5. *Dynamical instability against collapse*

For compact stars such as white dwarfs or neutron stars, we need to consider the stability of a single star to collapse. This instability sets in at the state of the maximum gravitational mass along the equilibrium sequence with the same distribution of the specific angular momentum for barotropes in Newtonian gravity.[3] (In general relativity situation is somewhat different.[4]) The criterion of this instability can be written as follows:

$$\rho_{\rm max} > \rho_{\rm max,c} \quad , \tag{2·12}$$

where $\rho_{\rm max}$ and $\rho_{\rm max,c}$ are the maximum density of the star and the density for the maximum gravitational mass state, respectively. It is not easy to find this critical configuration exactly because the equilibrium sequences for compact binary star systems are not those with the distribution of the specific angular momentum kept constant. However, roughly speaking, if the maximum density of the star increases as the separation decreases, there arises a possibility of onset of this instability for each component star.

2.6. *General relativistic instability*

In this paper, although we treat equilibrium configurations only in Newtonian gravity, we should point out that there is a critical state due to general relativistic instability of the orbital motion, i.e. the innermost stable circular orbit. The critical separation or the distance for this instability is denoted as $A_{\rm GR}$ or $d_{\rm GR}$. Here

$$d_{\rm GR} = 6M_{\rm tot} + \Delta \quad , \tag{2·13}$$

where $M_{\rm tot}$ is the total mass and Δ is a positive quantity which depends on the general relativistic structure of the system.

2.7. *Classification of binary equilibrium sequences by critical states*

By considering the order of appearance of these critical points along the equilibrium sequence, we can classify the quasi-stationary evolution of binary star systems into three types with several subtypes from the topology of the equilibrium sequence on the total angular momentum – separation plane.

Type 1a: The equilibrium sequence terminates at either A_c or $A_{\rm OF}$. There is no turning point.

Type 1b: The equilibrium sequence terminates at $A_{\rm RL}$. There is no turning point.

Type 2: The equilibrium sequence terminates at either A_c, $A_{\rm OF}$ or $A_{\rm RL}$ but the first critical point along the equilibrium sequence is the turning point. Thus the following condition is satisfied: $A_{\rm dyn} > A_c, A_{\rm OF}, A_{\rm RL}$.

Type 3: The equilibrium sequence terminates at either A_c or $A_{\rm OF}$. The first critical point along the equilibrium sequence is the turning point. Thus the following condition is satisfied: $A_{\rm dyn} > A_{\rm RL}$.

For quasi-stationary evolution of Type 1a, the final outcome is a single star or mass overflow from one component star to the other. For stars of Type 1b, 2 and 3, they suffer from dynamical disruption eventually. Of course, if the turning points are those for secular instability, stars will excite internal motion due to viscosity and can come closer. However, at the end they will finally encounter the turning point where dynamical instability sets in and suffer from dynamical disruption. Schematic figures of these types are shown in Fig. 4. Almost the same analysis has been done by Lai, Rasio and Shapiro.[7)]

§3. Classical results for binary star systems

Until early of 1980s, it was hard to obtain binary configurations of compressible gases. Therefore, structures of binary star systems had been investigated by assuming that 1) the density is constant, that 2) the shape of the star is ellipsoid, that 3) the angular velocity is constant and that 4) the vorticity is also constant. Under these assumptions three kinds of classical ellipsoids for binary star systems have been solved (see e.g. Ref. 5).

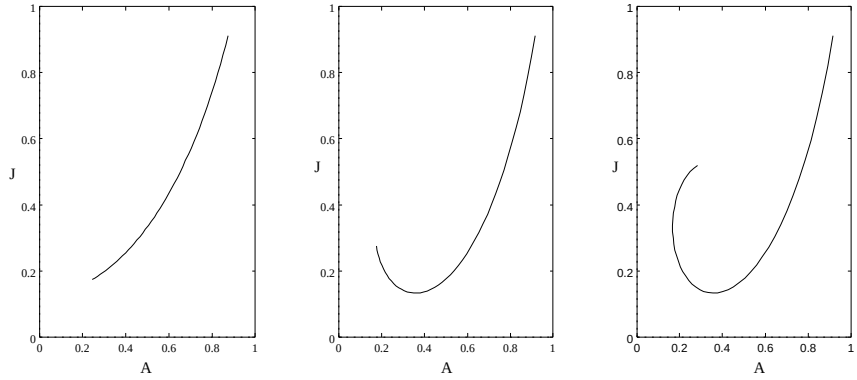

Fig. 4. The total angular momentum is plotted against the separation for equilibrium sequences which belong to Type 1 (left panel), Type 2 (middle panel) and Type 3 (right panel). The Type 1 equilibrium sequence terminates at either the contact state, the Roche lobe overflow state (Type 1a) or the Roche limit state (Type 1b). The Type 2 equilibrium sequence terminates at the contact state, the Roche lobe overflow state or the Roche limit state but there is a turning point along the sequence. The Type 3 equilibrium sequence terminates at the contact state or the Roche lobe overflow state. There is a turning point along the sequence. The Roche limit state comes between these critical configurations.

3.1. *Roche ellipsoid: synchronously rotating sphere (or point mass) – ellipsoid system*

Let us assume that one of the stars is a point mass or a sphere and that the other star is synchronously rotating with the orbital motion. If we include only the leading term of the tidal force from the point mass or the spherical star, the equilibrium condition for the fluid star can be expressed as

$$\frac{p}{\rho} = -\phi_1 + \frac{GM_2}{A^3}\left(x^2 - \frac{1}{2}y^2 - \frac{1}{2}z^2\right) + \frac{1}{2}\Omega^2(x^2+y^2) + \text{constant} \quad , \tag{3·14}$$

where p, ϕ_1, M_2 are the pressure, the gravitational potential of the fluid star (self-gravity) and the mass of the spherical star, respectively. The Cartesian coordinates (x, y, z) are used. If the shape of the fluid star is ellipsoid, this equilibrium condition can be satisfied by choosing the angular velocity Ω appropriately. This ellipsoid is called the Roche ellipsoid.

For the Roche ellipsoids with $M_1 = M_2$, the angular momentum – separation relation is shown in Fig. 5. As seen from this figure, the Roche ellipsoidal sequence belongs to Type 3. The curve of the spin angular momentum shows a turnaround due to a significant change of the internal structure. Along this sequence there appears a turning point where secular instability sets in. At this turning point the shape of ellipsoid is specified by $a_2/a_1 = 0.65$ and $a_3/a_1 = 0.59$ where (a_1, a_2, a_3) are three principal axis distances of the ellipsoid.

3.2. *Darwin ellipsoid: synchronously rotating congruent ellipsoids*

If two fluid stars are congruent and synchronously rotating, the equilibrium condition can be expressed as follows:

$$\frac{p}{\rho} = -\phi_1 + (\beta_1 x^2 + \beta_2 y^2 + \beta_3 z^2) + \frac{1}{2}\Omega^2(x^2+y^2) + \text{constant} \quad , \tag{3·15}$$

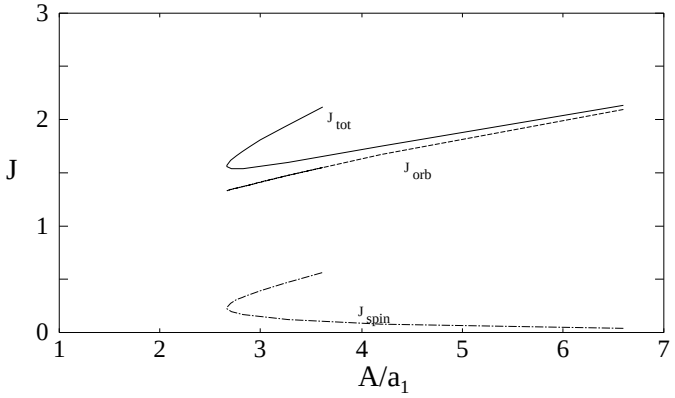

Fig. 5. Angular momentum is plotted against the separation for Roche ellipsoids. The orbital angular momentum (dashed curve), the spin angular momentum (dash-dotted curve) and the total angular momentum (solid curve) are shown. The turnaround of the spin curve is due to changes of the internal structure.

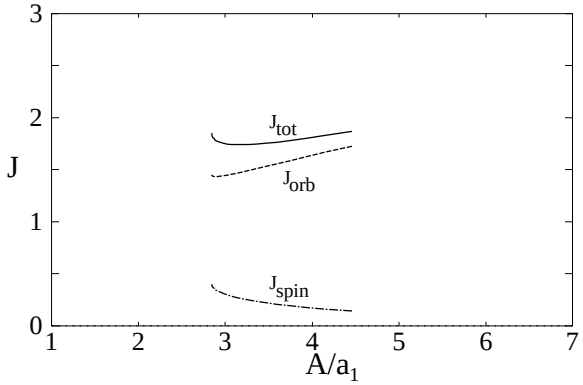

Fig. 6. Same as Fig. 5 but for Darwin ellipsoids. There is no turnaround of the spin curve.

where β's are constants which can be determined from the leading term of the tidal force from the secondary star. For this case, the ellipsoidal configuration satisfies the above equilibrium condition. Solutions to this equation are called Darwin ellipsoids. The equilibrium sequence is shown in Fig. 6. The sequence terminates at the contact state. Thus the Darwin sequence belongs to Type 3 sequence. The Roche limit state is characterized by $a_2/a_1 = 0.62$ and $a_3/a_1 = 0.56$.

3.3. *Roche-Riemann ellipsoid: a sphere (or point mass) – ellipsoid system with vorticity*

Fluid binary stars with nonzero vorticity were first investigated by Aizenman.[6] The system is almost the same as the Roche problem but in the fluid star there exist internal motions represented by the vorticity. The equilibrium condition is written as follows:

$$\frac{p}{\rho} = -\phi_1 - \phi_2 + \frac{1}{2}\Omega^2(x^2+y^2) + \frac{1}{2}u^2 + (2\Omega+\zeta)\Psi + \text{constant} \quad , \tag{3·16}$$

where ϕ_2, u and Ψ are the gravitational potential from the spherical star, the velocity of the internal motion in the rotating frame and the stream function of the internal motion,

respectively. This condition can be satisfied by ellipsoids and ellipsoidal solutions are called Roche-Riemann ellipsoids. According to the results of Aizenman, by introducing the internal flows, the minimum separation, i.e. Roche limit, can become smaller than hat for the Roche ellipsoids. In other words, two stars can come closer each other.

§4. Recent results for binary star systems in Newtonian gravity

Although basic properties of binary star systems have been understood by using classical results mentioned in the previous section, several crucial things have remained to be investigated. First, the constant density assumption is not valid for realistic binary stars. Second, the real shape of deformed stars is not ellipsoidal. Therefore we need to take these points into account to understand realistic evolution of compact binary star systems.

4.1. *Ellipsoidal approach*

The effect of the compressibility is introduced by Lai, Rasio and Shapiro.[7] They have investigated polytropic binary star systems:

$$p = K\rho^{1+1/n} \quad , \tag{4·17}$$

where K and n are a polytropic constant and the polytropic index, respectively. Concerning the shape of binary stars, they have assumed that it is approximated by ellipsoidal shape. By using the energy variational principle, they have obtained approximated equilibrium configurations.

Their main results are as follows. For simplicity we will call Roche or Roche-Riemann ellipsoids for the systems consisting of a spherical star (or point mass) and a compressible ellipsoid without or with internal motions, respectively. Darwin or Darwin-Riemann ellipsoids are used for the compressible congruent stars without or with internal motions.

For Roche and Roche-Riemann ellipsoids,

$$A_{\rm dyn} > A_{\rm RL} \quad . \tag{4·18}$$

This means that for these binary systems secular instability (Roche ellipsoids) or dynamical instability (Roche-Riemann ellipsoids) sets in before the Roche limit states are reached.

For Darwin ellipsoids, there is a critical value of the polytropic index as follows:

$$n^{\rm D}_{\rm cr} \approx 2 \quad , \tag{4·19}$$

and

$$\text{for} \quad n < n^{\rm D}_{\rm cr}, \quad A_{\rm dyn} > A_c \quad , \tag{4·20}$$

$$\text{for} \quad n \gtrsim n^{\rm D}_{\rm cr}, \quad A_c \ \text{comes first (no } A_{\rm dyn}) \quad . \tag{4·21}$$

This means that for rather stiff equations of state ($n < n^{\rm D}_{\rm cr}$) synchronously rotating compressible binary star systems suffer from secular instability and develop internal motions. However, for soft equations of state, stars come to contact without suffering from any critical phenomena.

For Darwin-Riemann ellipsoids, the situation is as follows. The critical polytropic index for the Darwin-Riemann ellipsoids is

$$n_{\rm cr}^{DR} \approx 1.2 \quad , \tag{4·22}$$

and

$$\text{for} \quad n < n_{\rm cr}^{\rm DR}, \quad A_{\rm dyn} > A_c \quad , \tag{4·23}$$

$$\text{for} \quad n \gtrsim n_{\rm cr}^{\rm DR}, \quad A_c \ \text{comes first (no } A_{\rm dyn}) \quad . \tag{4·24}$$

Thus for rather stiff binary stars ($n < n_{\rm cr}^{\rm DR}$) dynamical disruption would occur.

4.2. *Numerical solutions to exact basic equations for binary configurations in Newtonian gravity*

Very recently *exact equations* for binary configurations in Newtonian gravity have been numerically solved by us.[8] In our treatment, we assume 1) the polytropic equation of state, 2) the stationary state in the rotating frame, 3) inviscid fluid and 4) irrotational flows in the inertial frame. We do not assume the shape of configurations but we solve for the shape of configurations together with other quantities.

Basic equations are written as follows:

$$\int \frac{dp}{\rho} + \phi + \frac{1}{2}|\nabla\Psi|^2 - (\boldsymbol{\Omega} \times \boldsymbol{r})\nabla\Psi = constant \quad , \tag{4·25}$$

$$\phi = -\int \frac{\rho(\boldsymbol{r}')}{|\boldsymbol{r} - \boldsymbol{r}'|} d^3\boldsymbol{r}' \quad , \tag{4·26}$$

$$\Delta\Psi = n(\boldsymbol{\Omega} \times \boldsymbol{r} - \nabla\Psi) \cdot \frac{\nabla\Theta}{\Theta} \quad , \tag{4·27}$$

where Θ is defined as

$$p = K\Theta^{1+n} \quad . \tag{4·28}$$

Boundary conditions for these equations are as follows:

$$\Theta(r_s(\theta, \varphi)) = 0 \ \text{ for the matter} \quad , \tag{4·29}$$

$$\boldsymbol{n}_s \cdot \boldsymbol{v}_s = 0 \ \text{ for the flow} \quad , \tag{4·30}$$

where $r = r_s(\theta, \varphi)$, $\boldsymbol{n}_s$ and $\boldsymbol{v}_s$ are the surface of the star, the normal vector to the surface and the velocity vector along the surface, respectively.

In order to show only the effect of the shape and the structure, we will present the results for $n = 0$ polytropes or incompressible fluids. In Figs.7-8, results from the ellipsoidal approximation[7] and those of numerical computations[8] are shown. As seen from these figures, the exact treatment gives larger values of the moment of inertia and so the separation at the turning point shifts to larger value compared with that of the ellipsoidal approximation.

For numerical solutions of irrotational Darwin-Riemann compressible configurations, there is a critical polytropic index $n_{\rm cr}^{\rm eDR}$ as seen in Fig.9 (eDR means "exact" Darwin-Riemann). Therefore, irrotational polytropic binary star systems can be clas-

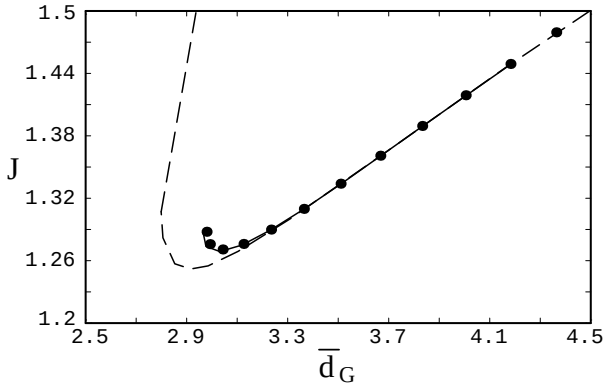

Fig. 7. The total angular momentum – separation relation for the irrotational Roche-Riemann incompressible sequence. The result from the ellipsoidal approximation[7] (dashed curve) and that of numerical computations[8] (solid curve and dots) are shown. The solid curve and the dots are computed by independent numerical methods.

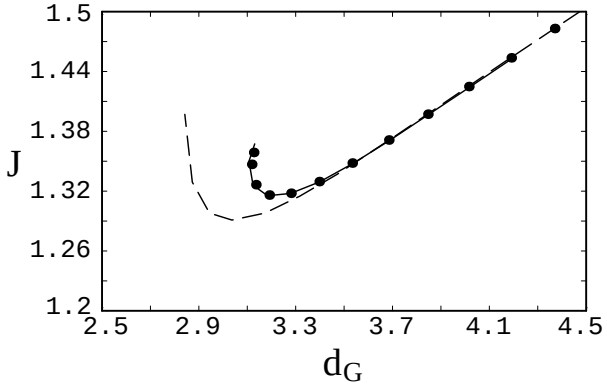

Fig. 8. Same as Fig.7 but for the irrotational Darwin-Riemann incompressible sequence.

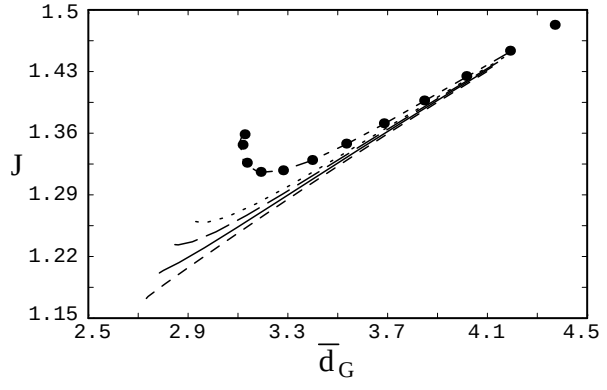

Fig. 9. The total angular momentum – separation relations for several polytropes of irrotational Darwin-Riemann sequences. Polytropes with $n = 0.0$ (dash-dotted), $n = 0.5$ (dotted), $n = 0.7$ (long dashed), $n = 1.0$ (solid) and $n = 1.5$ (short dashed) are shown.

sified as follows:

$$n_{\rm cr}^{eDR} \approx 0.7 \quad , \tag{4·31}$$

and

$$\text{for} \quad n < n_{\rm cr}^{\rm eDR}, \quad A_{\rm dyn} > A_{\rm OF} \quad , \tag{4·32}$$

$$\text{for} \quad n \gtrsim n_{\rm cr}^{\rm eDR}, \quad A_{\rm OF} \quad \text{comes first (no} \quad A_{\rm dyn}) \quad . \tag{4·33}$$

As discussed before, the critical value $n_{\rm cr}^{\rm eDR} \approx 0.7$ is much smaller than the critical value $n_{\rm cr}^{\rm DR} \approx 1.2$ obtained from the ellipsoidal approximation. This is an important difference because the effective polytropic index for realistic neutron stars is estimated $0.5 \sim 1.0$. Thus realistic neutron stars may not suffer from dynamical instability during evolution due to gravitational wave emission but result in mass overflow.

As for the numerical solutions of irrotational Roche-Riemann compressible configurations, critical polytropic indices $n_{\rm cr}^{\rm eRR}$ depend on the mass ratio of the stars. When $n > n_{\rm cr}^{\rm eRR}$, there appear no turning points and so binary star systems would result in mass overflow. If $n \lesssim n_{\rm cr}^{\rm eRR}$, turning points appear and dynamical disruption would occur. In Fig.10, the critical polytropic index is shown for different mass ratios for irrotational Roche-Riemann compressible binary star systems. This result is clear contrast to that of the ellipsoidal approximation because solutions from the ellipsoidal approximation always give a turning point along the sequences as shown in Fig.11.

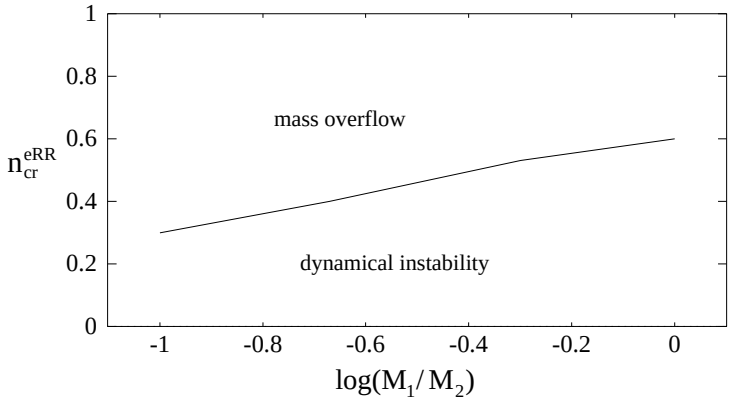

Fig. 10. The critical polytropic index is plotted against the mass ratio $\log(M_1/M_2)$ for irrotational Roche-Riemann compressible configurations. If the polytropic index is smaller than the critical polytropic index, the polytropic star would reach dynamically unstable state and disruption would occur. If the polytropic index is larger than the critical value, the mass overflow to the other star would begin.

§5. Discussion and Summary

5.1. *Discussion*

In this paper we have focused on the equilibrium sequences of binary star systems in Newtonian gravity. However, for compact binary star systems such as neutron star – neutron star binary systems or neutron star – black hole binary systems, the role of general relativity is important. The internal structure and the orbital nature are

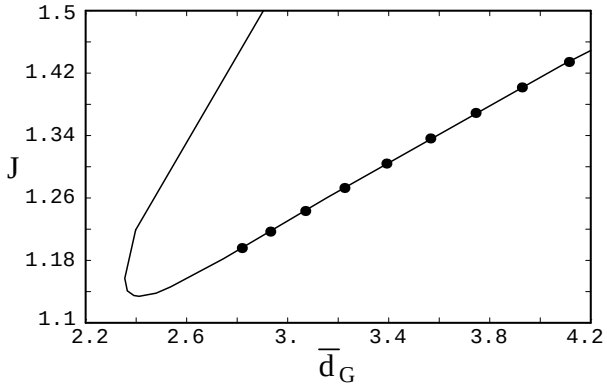

Fig. 11. Same as Fig.7 but for the irrotational Roche-Riemann $n = 1$ polytropic sequence. The results from the ellipsoidal approximation[7] (solid curve) and that of numerical computations[8] (dots) are shown.

affected by general relativity. Concerning the internal structure, general relativity tends to make the matter softer or increase the "effective" polytropic index so that the mass will concentrate towards the central region. This implies that mass overflow will be more likely to occur.

As for the orbital motion, from the perturbative analysis of the black hole – neutron star binary system, the following relation for the innermost stable circular orbit has been obtained:[9, 10]

$$d_{\rm GR} = 6M_{\rm tot} + 4\mu \quad , \tag{5·34}$$

where μ is the reduced mass:

$$\mu \equiv= \frac{M_1 M_2}{M_1 + M_2} \quad . \tag{5·35}$$

From this radius, we can roughly estimate that

$$d_{\rm OF}(\approx d_{\rm RL}) > d_{\rm GR} \ , \quad \text{for} \ \ \frac{M_1}{M_2} \gtrsim 0.25, \ 0.5 \lesssim n \lesssim 1.0 \ \text{and} \ \frac{M_1}{R_*} \lesssim 0.15 \quad . \tag{5·36}$$

This means that the mass overflow radius is reached before the general relativistic effect begins to work.

Concerning the critical radius of the dynamical instability, Shibata[11] has shown by using the post-Newtonian approximation that

$$d_{\rm dyn} \ (\text{for post} - \text{Newtonian case}) < d_{\rm dyn} \ (\text{for Newtonian case}) \quad . \tag{5·37}$$

Thus the qualitative results about the critical radii obtained from the Newtonian analysis would not be changed even in general relativistic analysis, although the values are necessarily different.

We need to comment on the behavior of the maximum density of the individual star along the quasi-stationary evolutionary sequence. In general relativistic computations, Wilson, Mathews and Maronetti[12] have shown that the maximum density increases as the system evolves. However, recently, Bonazzola, Gourgoulhon and Marck[13] and Uryu and Eriguchi[14] have shown that the central density of the component star of the irrotational binary star systems in general relativity decreases as the binary star

system evolves, although at large separations there is some stage where the central density increases slightly.

Our Newtonian computations also show that the maximum density decreases as evolution proceeds. This is shown in Fig.12. For Newtonian polytropes, Taniguchi

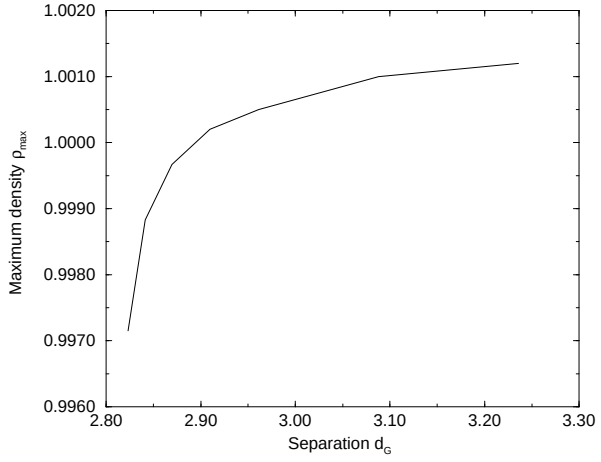

Fig. 12. The maximum density is plotted against the separation for $n = 1$ irrotational Darwin-Riemann configuration systems. The maximum density is normalized by the maximum density of the spherical star.

and Nakamura[15] have analyzed irrotational binary star systems of $n = 1$ polytropes perturbationally and found that

$$\left(\frac{\rho_{\rm max,i} - \rho_{\rm max}}{\rho_{\rm max,i}}\right) = \frac{45}{2\,(M_1/M_2)^2\,\xi_1^2}\left(\frac{a_0}{A}\right)^6 \quad , \tag{5·38}$$

to the order of $\mathcal{O}(1/A^6)$, where $\rho_{\rm max,i}$ and a_0 are the maximum density and the radius for the initial spherical star, respectively. Here ξ_1 equals to π for $n = 1$ case. Therefore, it is very likely that the maximum mass will not increase significantly. In other words, the component star would not suffer from dynamical instability to collapse.

5.2. *Summary*

We have reviewed properties of classical and/or approximated equilibrium sequences of Darwin, Darwin-Riemann, Roche and Roche-Riemann problems in Newtonian gravity in the context of the final evolution of compact binary star systems due to gravitational wave emission.

We have presented the results of full numerical computations of equilibrium sequences of irrotational binary star systems in Newtonian gravity. From the analysis of critical points along these equilibrium sequences, we have shown the possibility that evolution of compact binary neutron star systems would result in mass overflow instead of dynamical disruption for a certain parameter ranges.

Acknowledgements

A part of the numerical computations has been carried out at the Astronomical Data Analysis Center of the National Astronomical Observatory, Japan. One of us (KU) would like to thank Prof. J.C. Miller for discussions and continuous encouragements. He would also like to thank Prof. D.W. Sciama and A. Lanza for his warm hospitality at SISSA and ICTP.

References

1) C.S. Kochanek, Astrophys. J. **398** (1992), 234.
2) L. Bildsten and C. Cutler, Astrophys. J. **400** (1992), 175.
3) G.S. Bisnovatyi-Kogan and S.I. Blinnikov, Astron. Astrophys. **31** (1974), 391.
4) J.L. Friedman, J. Ipser and R.D. Sorkin, Astrophys. J. **325** (1988), 722.
5) S. Chandrasekhar, *Ellipsoidal Figures of Equilibrium* (Yale University Press, New Haven, 1969).
6) M.L. Aizenman, Astrophys. J. **153** (1968), 511.
7) D. Lai, F.A. Rasio and S.L. Shapiro, Astrophys. J. Suppl. **88** (1993), 205; Astrophys. J. **406** (1993), L64; Astrophys. J. **420** (1994), 420; Astrophys. J. **423** (1994), 344.
8) K. Uryū and Y. Eriguchi, Mon. Not. Roy. Astron. Soc. **296** (1998), L1; Astrophys. J. Suppl. **118** (1998), 563; Mon. Not. Roy. Astron. Soc. **299** (1998), 575; Mon. Not. Roy. Astron. Soc. **303** (1999), 329.
9) L.E. Kidder, C.M. Will and A.G. Wiseman, Class. Quantum Gravity **9** (1992), L125.
10) D. Lai, F.A. Rasio and S.L. Shapiro, Astrophys. J. **420** (1994), 811.
11) M. Shibata, Phys. Rev. **D55** (1997), 6019.
12) J.R. Wilson, G.A. Mathews and P. Maronetti, Phys. Rev. **D54** (1996), 1317.
13) S. Bonazzola, E. Gourgoulhon and J.-A. Marck, Phys. Rev.Lett. **82** (1999), 892.
14) K. Uryū and Y. Eriguchi, Phys. Rev. (1999), submitted (gr-qc/9908059).
15) K. Taniguchi and T. Nakamura, Phys. Rev.Lett. (1999), submitted.